Title

CWAS-Plus: estimating category-wide association of rare noncoding variation from whole-genome sequencing data with cell-type-specific functional data.

Permalink

Journal

Authors

Kim, Yujin
Jeong, Minwoo
Koh, In
et al.

Publication Date

DOI

CWAS-Plus: estimating category-wide association of rare noncoding variation from whole-genome sequencing data with cell-type-specific functional data

Yujin Kim[1,2,‡], Minwoo Jeong[3,‡], In Gyeong Koh[1,2], Chanhee Kim[1,2], Hyeji Lee[1,2], Jae Hyun Kim[1,2], Ronald Yurko [4], Il Bin Kim[5],

Jeongbin Park[6], Donna M. Werling[7], Stephan J. Sanders[8,9], Joon-Yong An [1,2,3,*]

[1]Department of Integrated Biomedical and Life Science, Korea University, 145 Anam-ro, Seongbuk-ku, Seoul 02841, Republic of Korea
[2]L-HOPE Program for Community-Based Total Learning Health Systems, Korea University, 145 Anam-ro, Seongbuk-ku, Seoul 02841, Republic of Korea
[3]School of Biosystem and Biomedical Science, College of Health Science, Korea University, 145 Anam-ro, Seongbuk-ku, Seoul 02841, Republic of Korea
[4]Department of Statistics and Data Science, Carnegie Mellon University, 5000 Forbes Avenue, Squirrel Hill North, Pittsburgh, PA 15213, United States
[5]Department of Psychiatry, CHA Gangnam Medical Center, CHA University School of Medicine, 566 Nonhyon-ro, Gangnam-gu, Seoul 06135, Republic of Korea
[6]School of Biomedical Convergence Engineering, Pusan National University, 49 Busandaehak-ro, Mulgeum-eup, Yangsan-si, Gyeongsangnam-do, 50612, Republic of Korea
[7]Laboratory of Genetics, University of Wisconsin-Madison, 425-g Henry Mall, Madison, WI 53706, Unite States
[8]Department of Paediatrics, Institute of Developmental and Regenerative Medicine, University of Oxford, Old Road Campus, Roosevelt Dr, Headington, Oxford OX3 7TY, United Kingdom
[9]Department of Psychiatry and Behavioral Sciences, UCSF Weill Institute for Neurosciences, University of California, 1651 4th Street, San Francisco, CA 94158, United States

*Corresponding author. School of Biosystem and Biomedical Science, College of Health Science, Korea University, Seoul 02841. E-mail: joonan30@korea.ac.kr
‡Yujin Kim and Minwoo Jeong Joint Authors.

Abstract

Variants in *cis*-regulatory elements link the noncoding genome to human pathology; however, detailed analytic tools for understanding the association between cell-level brain pathology and noncoding variants are lacking. CWAS-Plus, adapted from a Python package for category-wide association testing (CWAS), enhances noncoding variant analysis by integrating both whole-genome sequencing (WGS) and user-provided functional data. With simplified parameter settings and an efficient multiple testing correction method, CWAS-Plus conducts the CWAS workflow 50 times faster than CWAS, making it more accessible and user-friendly for researchers. Here, we used a single-nuclei assay for transposase-accessible chromatin with sequencing to facilitate CWAS-guided noncoding variant analysis at cell-type-specific enhancers and promoters. Examining autism spectrum disorder WGS data ($n = 7280$), CWAS-Plus identified noncoding

Yujin Kim is a graduate student at Korea University, where she focuses on studying noncoding variants that disrupt enhancers implicated in autism and developing a statistical method for the genetic association of rare variants from whole-genome sequencing data.
Minwoo Jeong worked as a research assistant with a particular interest in developing bioinformatic methods for large-scale whole-genome sequencing projects.
In Gyeong Koh a graduate student at Korea University, is currently engaged in developing a single-cell sequencing atlas and data integration methods for various human brain transcriptome studies.
Chanhee Kim is a graduate student at Korea University studying rare noncoding variants in Alzheimer's disease using category-wide association techniques and applying them to large-scale whole-genome sequencing studies of Alzheimer's disease.
Hyeji Lee is a graduate student at Korea University and focuses on studying rare inherited variants in autism and neurodegenerative disorders.
Jae Hyun Kim formerly a graduate student at Korea University, conducted research on noncoding structural variants in autism using whole-genome sequencing datasets.
Ronald Yurko is an assistant teaching professor in the Department of Statistics & Data Science at Carnegie Mellon University. Dr. Yurko is interested in developing methods at the interface of inference and machine learning, particularly oriented toward problems in statistical genetics and genetic association studies.
Il Bin Kim a professor at the Department of Psychiatry, CHA University School of Medicine, is dedicated to psychiatric genetics and the identification of promoter-enhancer interactions in the noncoding genome from a whole-genome sequencing study of Korean autism families (Kim et al., 2022, Molecular Psychiatry).
Jeongbin Park an assistant professor at the School of Biomedical Convergence Engineering, Pusan National University, focuses on developing machine learning and probabilistic tools for various genomic studies and has contributed to the development of various packages for single-cell analysis.
Donna M. Werling an assistant professor at the University of Wisconsin-Madison, conducts research on genetic risk factors for autism and other neuropsychiatric conditions, as well as sex differences in neurobiology and disease risk. Dr. Werling has developed bioinformatics tools, including the category-wide association test, for large-scale whole-genome sequencing studies (Werling et al., 2018, Nature Genetics) and identified regulatory noncoding variants associated with human cortical development (Werling et al., 2020, Cell Reports).
Stephan J. Sanders a professor at the Department of Paediatrics, University of Oxford, and the Department of Psychiatry and Behavioral Sciences, University of California, San Francisco, is renowned for his landmark studies on *de novo* variants in autism (Sanders et al., 2012, Nature), autism-associated genes (Sanders et al., 2015, Neuron), and noncoding risk mutations in autism (An et al., 2018, Science).
Joon-Yong An an associate professor at the Department of Biosystem and Biomedical Science at Korea University, has been dedicated to autism genetics and large-scale whole-genome sequencing analysis. Dr. An introduced the category-wide association test method for whole-genome sequencing studies (Werling et al., 2018) and identified noncoding risk mutations in autism (An et al., 2018, Science).

de novo variant associations in transcription factor binding sites within conserved loci. Independently, in Alzheimer's disease WGS data ($n = 1087$), CWAS-Plus detected rare noncoding variant associations in microglia-specific regulatory elements. These findings highlight CWAS-Plus's utility in genomic disorders and scalability for processing large-scale WGS data and in multiple-testing corrections. CWAS-Plus and its user manual are available at https://github.com/joonan-lab/cwas/ and https://cwas-plus.readthedocs.io/en/latest/, respectively.

Graphical Abstract
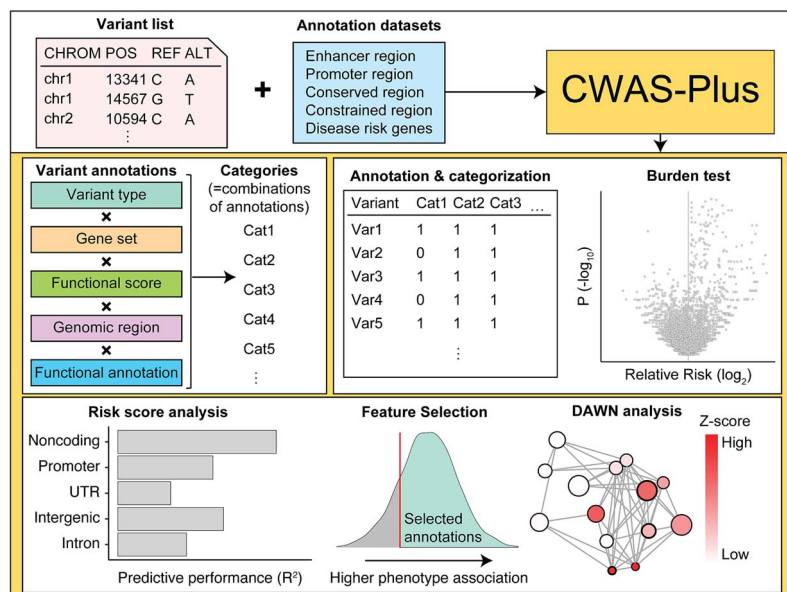
Keywords: genetic association; whole-genome sequencing; regulatory noncoding variant; rare variant; noncoding genome

Introduction

The noncoding regions of the genome contain key regulatory elements, including promoters and enhancers, which are essential for tissue-specific gene expression and play a vital role in cellular and organ development during early human development [1, 2]. Recent large-scale single-cell assays for transposase-accessible chromatin with sequencing (ATAC-Seq) studies have identified cell type-specific noncoding elements at critical developmental milestones and profiled key regulatory enhancers of gene expression dynamics [3, 4]. Disruption of these elements by genetic variants may alter gene expression in biological pathways and consequently lead to human disorders [5–7]. Notably, most of the associations from genome-wide association studies (GWAS) are in noncoding regions enriched for regulatory elements [8, 9], highlighting the importance of identifying variants within these key regulatory elements in the noncoding sequences to gain critical insights into genetic disorders.

Recent advances in whole-genome sequencing (WGS) have enabled the identification and risk evaluation of rare noncoding variants for disorders [10, 11]. Several methods prioritize high-risk noncoding variants (RNVs) using scoring systems based on functional annotations but lack statistical evaluation for genome-wide associations [12–19]. With the growing volume of WGS data, new methods have emerged for genome-wide genetic association studies of noncoding variants, focusing on functional regions [20] or predefined genomic windows [21]. Phenotype–genotype association studies with functional regions have also been introduced [22]. Recently, we developed the category-wide association study (CWAS), a novel statistical framework to identify noncoding associations from WGS data [23]. This method utilizes variant groups, called categories, for genetic association testing and creates multiple categories based on genomic and functional annotations

related to noncoding variants. Traditional GWAS assess associations at the locus level, which can result in insufficient statistical significance for rare variants. CWAS addresses this limitation by conducting association tests on categorized variants, making it applicable for rare variants. With CWAS, we have successfully identified that noncoding variants in conserved regions of promoters are significantly enriched for autism spectrum disorder (ASD) [24].

Herein, we introduce CWAS-Plus, a Python package that enhances CWAS for identifying genetic associations among noncoding variants. CWAS-Plus significantly reduces run time and computational requirements, resulting in faster and more efficient execution of the entire CWAS workflow. CWAS-Plus integrates multiple datasets to define functional regions or genes of interest provided by the users as bed files or gene sets. Additionally, it introduces a novel approach for multiple-testing corrections, further enhancing the reliability of the results. We applied CWAS-Plus to large-scale WGS datasets and, through the integration of single-cell datasets, found that ASD noncoding association disrupts transcriptional regulation. Furthermore, applying CWAS-Plus to rare variants identified microglia-specific noncoding associations with Alzheimer's disease (AD). Taken together, we highlight the potential of CWAS-Plus for discovering noncoding risks from WGS data across various disorders.

Methods
Input requirement

CWAS-Plus requires a list of variants and samples for association testing. For the variant list, Variant Call Format (VCF) is used to include genomic position, reference allele, alternate allele, and

sample identification (ID). A sample list should contain sample IDs and phenotypic labels (e.g. case or control). These inputs are subject to variant annotation for genomic regions using the Variant Effect Predictor (VEP) [25].

Users can provide adjustment factors to correct for confounding factors in the analysis. CWAS-Plus uses these adjustment factors by multiplying them by the number of variants for each sample. In our analyses, since the number of *de novo* variants increases with paternal age [26, 27], we adjusted for paternal ages and sample cohorts to remove biases (see 'Adjustment factors for *de novo* variants' section in Supplementary Materials for detailed methods).

Annotation

The variant annotation process involves two steps: the VEP annotation and the customized annotation. VEP annotates the most severe consequence using Sequence Ontology (SO) terms, which are then employed for categorizing genomic regions. In this study, VEP version 110 was used. Customized annotation was conducted for user-provided datasets, including functional annotation and functional score. Functional annotation refers to specific genomic regions associated with particular functions, such as epigenetic status. Functional scores indicate regions with score metrics related to genomic features, such as conservation.

Categorization

To assess the noncoding association, CWAS-Plus creates categories for variants using genomic and functional annotations. A single category is built by combining five features: (i) variant type, (ii) genomic region, (iii) gene set, (iv) functional annotation, and (v) functional score (see 'Annotation datasets used in CWAS analysis' section in Supplementary Materials for datasets used in each feature). Among the five features, gene set, functional annotation, and functional score features are user-provided datasets.

(1) Variant type: variants are classified into either single nucleotide variant (SNV) or insertion–deletion (indel) based on the length of the alleles.
(2) Genomic region: genomic region based on the location of the variant relative to genes. Genomic region is defined by utilizing SO terms from the most severe consequence and the annotated gene from VEP annotation. Genomic regions include coding domains [e.g. protein-truncating variants (PTVs), frameshift indels, missense, damaging missense, in frame indels, and silent variants] and noncoding domains (e.g. those composed of 5′ UTR, 3′ UTR, promoter, splice site, intron, intergenic, long noncoding RNA, and others), with the order corresponding to the order of variant annotation. PTVs (nonsense and frameshift) must have a high confidence level ('HC') using the LOFTEE plugin and be annotated with either 'SINGLE_EXON' or no LOFTEE flags. Damaging missense variants are required to have an MPC score of ≥ 2. Promoter variants are annotated as 2000 base pairs upstream of transcription start sites.
(3) Gene set: disease-relevant gene sets. Datasets should be in text format.
(4) Functional annotation: functional regions associated with epigenetic modifications or regulatory elements. Datasets should be in bed format.
(5) Functional score: score metrics related to specific genomic features, such as conservation or pathogenicity. Datasets should be in bed format.

Categories are constructed by grouping variants according to their respective annotations. Specifically, variants sharing annotations across five distinct features are consolidated into a single category. For instance, a category can be established containing intergenic SNVs near CHD8 target genes, located within excitatory neuron-specific *cis*-regulatory elements (CREs), and conserved genomic loci. Genetic variants exhibiting overlapping annotations across all these features are then assigned to this category.

Burden test

CWAS-Plus assesses the association within a single category by conducting burden tests through two approaches: variant-level and sample-level tests.

In the variant-level test, the case–control association is estimated by comparing the number of variants in each category. The relative risk (RR) is calculated using the following equation:

$$\text{Case ratio}_i = \frac{\text{Number of variants in cases within } i^{\text{th}} \text{ category}}{\text{Number of total cases}}$$

$$\text{Control ratio}_i =$$

$$\frac{\text{Number of variants in controls within } i^{\text{th}} \text{ category}}{\text{Number of total controls}}$$

$$\text{Relative Risk} = \frac{\text{Case ratio}_i}{\text{Control ratio}_i}.$$

The binomial *P*-value is calculated by comparing two proportions: variants in cases from total variants within a category and cases from total samples.

$$X_i = \text{Number of variants in cases within } i^{\text{th}} \text{ category}$$

$$N_i = \text{Number of variants within } i^{\text{th}} \text{ category}$$

$$p = \frac{\text{Number of cases}}{\text{Number of total samples}}$$

$$\text{Binomial test } (X_i, N_i, p)$$

$$X_i \sim b(N_i, p).$$

In the sample-level test, the case–control association is estimated by comparing the number of samples carrying variants in each category. The RR is calculated using the following equation:

$$\text{Case ratio}_i = \frac{\text{Number of cases within } i^{\text{th}} \text{ category}}{\text{Number of total cases}}$$

$$\text{Control ratio}_i = \frac{\text{Number of controls within } i^{\text{th}} \text{ category}}{\text{Number of total controls}}$$

$$\text{Relative Risk} = \frac{\text{Case ratio}_i}{\text{Control ratio}_i}.$$

The binomial *P*-value is calculated by comparing two proportions: cases from total samples within a category and cases from total samples

$$X_i = \text{Number of cases within } i^{\text{th}} \text{ category}$$

$$N_i = \text{Number of total samples within } i^{\text{th}} \text{ category}$$

$$p = \frac{\text{Number of cases}}{\text{Number of total samples}}$$

$$\text{Binomial test } (X_i, N_i, p)$$

$$X_i \sim b(N_i, p).$$

Case–control label-swapping permutations generate *P*-values in both tests.

During burden tests, CWAS-Plus can correct confounding factors by adjusting the number of variants per sample. In this study, *de novo* variant counts were corrected for paternal age at birth and sample cohorts.

Risk score analysis

Risk score analysis generates risk scores for each category to identify effective phenotype predictors. CWAS-Plus employed a Lasso regression model, focusing on rare categories (<2 variants in controls), and incorporated the number of variants in each category across samples as a metric. This metric served as training data for Lasso regression, with categories as features and disease phenotypes as labels. Through Lasso regression, CWAS-Plus identifies the categories that best predict case status and assigns coefficients, defined as risk scores, to each category.

In the analyses, 80% of samples ($n = 5824$ for variant-level analysis; $n = 869$ for sample-level analysis) constituted the training set. The optimal model was determined by testing 100 lambda values from five-fold cross-validation, repeated 10 times. The lambda yielding the minimum mean cross-validated error was selected to ensure generalizability and prevent overfitting. Model performance was evaluated using the *R*-squared (R^2) values, and significance was assessed by label-swapping 1000 times, randomly assigning phenotypes to samples.

The Lasso regression model formula can be defined as follows:

$$\min_{\beta} \left\{ \frac{1}{2n} \sum_{i=1}^{n} \left(y_i - x_i^T \beta \right)^2 + \lambda \sum_{j=1}^{p} |\beta_j| \right\}$$

where y_i is the observed phenotype, indicating case or control. x_i is the number of variants (or samples) in each category for each sample. β are the regression coefficients, and λ is the regularization parameter.

For feature selection, risk score analysis was applied to noncoding categories from each annotation dataset (i.e. gene set, functional annotation, and functional score). Datasets with positive R^2 values were further analyzed (see 'Risk score analysis' section in Supplementary Materials for detailed methods).

Burden shift analysis

CWAS-Plus identifies overrepresented annotations from category-level burdens. In each permutation ($n = 10\,000$), phenotypes are randomly assigned to samples while maintaining the original ratio. Subsequently, CWAS-Plus compares the number of significant categories of interest with those from each permutation, obtaining *P*-values for each phenotype.

Clustering of categories

CWAS-Plus clusters categories by calculating correlation values between two categories. The correlation is calculated based on the principle that, under the null hypothesis, the covariance is equivalent to the variance of shared variants [28]. Because a binomial random variable can be expressed as the sum of independent Bernoulli variables, the variance can be computed using the equation:

$$n \times p \times (1 - p)$$

where *n* represents the number of tests and *p* denotes the binomial probability, which is determined by the proportion of case samples among all samples.

Each variant is treated as an independent test, replacing the total number of tests (*n*) with the number of variants. Consequently, the covariance between two categories is determined by the number of shared variants. We obtained a correlation matrix of size $c \times c$ by calculating the standardized covariance for all pairs of categories among the total.

Finding the number of effective tests for burden test

To estimate the threshold for genome-wide significance, we converted the correlation matrix into a negative Laplacian metric. Initially, we transformed the correlation matrix into absolute values. Subsequently, we established a degree matrix by aggregating all correlation values for each category. Then, we divided the absolute correlation values by the squared values of the corresponding entries in the degree matrix, deriving the Laplacian matrix. Utilizing this matrix, eigen decomposition identified the number of eigenvalues explaining at least 99% of the variance, which determined the effective number of tests.

Detecting Association With Networks (DAWN) analysis

To investigate subnetworks within noncoding risk categories, we utilized the DAWN algorithm [29]. Metrics from risk-associated categories were converted into two-dimensional coordinates using *t*-distributed stochastic neighbor embedding (*t*-SNE), selecting the top 50 eigenvalues (excluding the first). These coordinates were clustered with *k*-means or Leiden methods, and disease associations were determined using a hidden Markov random field model. Permutation P-values were transformed into z-scores, and Sparse Principal Component Analysis identified key variants within each cluster. Clusters were considered significant (false discovery rate (FDR) $< 5.0 \times 10^{-2}$) if their z-scores indicated a non-random association with ASD. Variants from these significant clusters were classified as RNVs (see 'Detecting Association With Networks (DAWN) analysis' section in Supplementary Materials for detailed methods).

WGS datasets used in CWAS-Plus

For benchmarking CWAS-Plus, we used 255 106 *de novo* variants identified in 1902 ASD families from our previous WGS study [24].

For variant-level CWAS analyses, we obtained project VCF with joint genotyping in 4270 ASD families from the Simons Simplex Collection (SSC) [30] and Simons Foundation Powering Autism Research for Knowledge (SPARK) [31]. ASD families include 4354 ASD cases and 2926 unaffected control siblings. Data access and analyses were approved by the Institutional Review Board of Korea University (approval number: KUIRB-2022-0409-03). After quality control, 474 788 *de novo* variants identified from 7280 samples were utilized (see 'High quality variants for variant-level analyses' section in Supplementary Materials for detailed methods).

For sample-level CWAS analyses, we obtained 63 667 178 variants from 1196 individuals in the Religious Orders Study and the Memory and Aging Project (ROSMAP) study [32, 33]. After quality control, 25 052 701 variants from 1087 samples were utilized (see 'High quality variants for sample-level analyses' section in Supplementary Materials for detailed methods).

Downstream analysis
Transcription factor enrichment

We investigated the enrichment of human transcription factors ($n = 1622$) [34] in genes affected by RNVs, PTVs, and noncoding variants (excluding RNVs). The fisher's exact test, followed by

FDR correction, determined significance with an adjusted P-value threshold of $<5.0 \times 10^{-2}$. Background gene sets included all genes from GENCODEv44 and genes annotated to variants.

Correlation between DAWN clusters and single annotation datasets

To assess the correlation between DAWN clusters and single annotation datasets, we extracted variants from each cluster and annotation dataset. The correlation was calculated using the same method as in CWAS-Plus, where we determined the number of shared variants between two sets (either from clusters or single annotations), considering the number of variants in each set.

Comparison of CWAS-Plus with Sei, Enformer, and STAARpipeline

We compared CWAS-Plus, Sei [35], Enformer [36], and STAARpipeline [22] by analyzing 474 788 *de novo* variants from CWAS analyses. For Sei and Enformer, pretrained models were used. STAARpipeline was applied using the functional datasets from the variant-level CWAS analyses and the Functional Annotation of Variant–Online Resource (FAVOR) database [37], which STAARpipeline requires.

We evaluated the ability to prioritize ASD-specific risk variants by defining risk variant carriers and assessing their case-enrichment. In CWAS-Plus, risk variant carriers were samples with at least three RNVs identified in CWAS analyses. Among 40 sequence classes predicted by Sei, we focused on brain- and transcription-associated features, including TN, TF, P, CTCF groups, and brain-related E groups. For Enformer, we selected brain- and embryo-related features from the 5313 genomic tracks. For both Sei and Enformer, risk variant carriers were defined as samples with variants that exceeded absolute scores of 1.1 and 200, respectively, for each predicted feature. In STAARpipeline, carriers were defined as samples with variants from gene-centric noncoding analysis in protein-coding and noncoding RNA genes, respectively, with $P < 5.0 \times 10^{-2}$. Using these defined risk variant carriers from each tool, we calculated the odds ratio (OR) for cases and controls.

Results
Overview of the CWAS-Plus pipeline

The CWAS-Plus package includes several steps to explore the noncoding associations of genetic disorders (Fig. 1A). CWAS-Plus utilizes various datasets to annotate variants and extract relevant genomic information (Fig. 1B). The annotated information is employed for variant categorization, in which categories are defined by the combination of five features: variant type, genomic region, gene set, functional annotation, and functional score (Fig. 1B). Subsequently, association tests are conducted for each category (Fig. 1C). CWAS-Plus utilizes these associations from single categories to provide more comprehensive measurements with multiple categories, enhancing noncoding associations to identify variants contributing to disease risk more effectively.

With categorized variants, risk score analysis identifies categories that predict disease phenotypes (Fig. 1D). The predictive contribution of each category is assessed by a Lasso regression model using the category patterns of each sample. In risk score analysis, feature selection is conducted to select phenotype-relevant datasets with positive model performance (R^2) for further analyses. Subsequently, burden shift analysis identifies overrepresented annotations in category-level association tests (Fig. 1E).

Table 1. Comparison of CWAS-Plus and CWAS.

	CWAS	CWAS-Plus
RAM	$\geq$16 GB	$\geq$16 GB
Total execution time	142 h	170 min
Programming language	R, Python2	Python3
Packaging	No	Yes
Multiprocessing	Yes	Yes
Batching	No	Yes
Setting environment	n/a	Pip
Annotation harmonization support	No	Yes

Both tests were conducted using 36 cores and 256 GB of memory. n/a, not applicable.

The significant excess of association compared to the null distribution suggests disease risk. Comparing results from both analyses assesses signal concordance, yielding candidate categories for disease association and subsequent Detecting Association With Networks (DAWN) analysis. Furthermore, CWAS-Plus provides a reliable method (Fig. 1F) to determine the number of effective tests. By treating highly correlated categories as a single effective test, it facilitates an accurate estimation of the study's wide significance. In DAWN analysis, categories are clustered and investigated for associations with disease risk (Fig. 1G). Based on the DAWN algorithm [29], CWAS-Plus constructs a network of clusters and evaluates disease risk considering nearby clusters, enhancing the identification of variants with risk. Significant clusters yield RNVs, potential pathogenic variants with noncoding associations. To illustrate the overall workflow, we present a toy example showing a simple schematic view and the order of major computation steps in CWAS-Plus (Supplementary Fig. 1).

The CWAS-Plus pipeline, described above, receives a list of variants as input and comprises seven steps to assess the noncoding association. We performed variant-level analysis using *de novo* variants from 7280 samples in ASD families. Additionally, sample-level analyses utilized rare variants from 1087 WGS samples in the ROSMAP [32].

Performance improvements in CWAS-Plus

CWAS-Plus offers several advantages over CWAS [24] (Table 1), owing to its transformation into a user-friendly Python package with simplified source code. Researchers can easily employ its capabilities through straightforward parameter settings. The reorganization of the source code improves comprehensibility as well as enables streamlined multiprocessing, resulting in shorter processing times.

We benchmarked the performance of CWAS-Plus and compared a run time between CWAS-Plus and CWAS [24]. We performed the CWAS analysis for *de novo* variants of ASD families using the CWAS-Plus package and our previous CWAS scripts (https://github.com/sanderslab/cwas). For this, we obtained the annotation (total 27 462 categories) and sample dataset (1902 ASD cases and 1902 unaffected controls) from the previous study [24] and evaluated the comparison using the same computing resource (36 CPU threads and 256 GB of memory). CWAS-Plus was 50 times faster than CWAS, highlighting its superior computational speed (Fig. 2A, Supplementary Table 1).

We further assessed the computational efficiency of CWAS-Plus by examining its CPU and memory usage. We observed that CWAS-Plus operates efficiently with a single CPU, leading to reasonable execution times. For datasets with <27 000 categories, CWAS-Plus was sufficient with <16 GB of RAM,
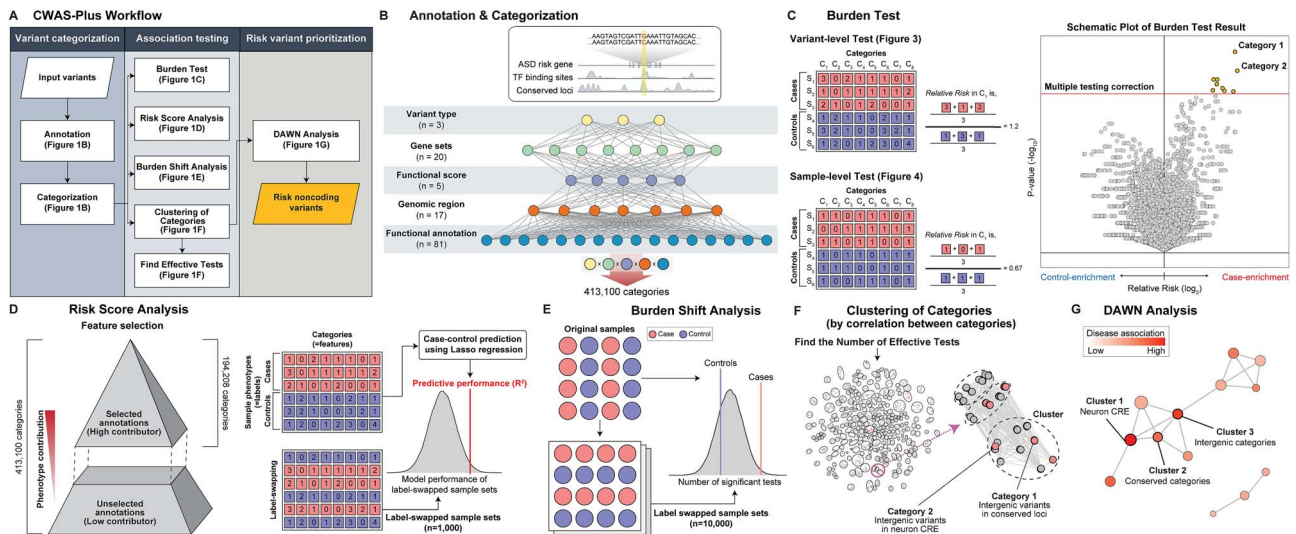
Figure 1. Overview of CWAS-Plus. (A) Overview of the CWAS-Plus workflow. (B) An example of annotation and categorization. (C) Burden test for a variant- and sample-level test: the number in the boxes indicates the number of variants in each category across samples. The volcano plot contains the burden test result for single categories. The x-axis indicates the RR in the $\log_2$ scale, whereas the y-axis indicates two-sided binomial P-values in the $\log_{10}$ scale. The dashed line indicates the study-wide significance threshold for the number of effective tests. (D) Risk score analysis: through feature selection, annotation datasets with high phenotype association are selected for further analyses. Label-swapping randomly assigns phenotypes to samples. The density plot displays the R^2 distribution of label-swapped samples ($n = 1000$). The line represents observed R^2 from the original samples. (E) Burden shift analysis: label-swapping assigns phenotypes randomly to samples. Circles represent samples. The density plot shows the distribution of significant category counts for label-swapped samples, with observed significant category counts depicted as lines. (F) Find the number of effective tests: Categories are clustered based on pairwise correlations to determine the number of effective tests. Each dot represents a category, with circles indicating clusters. The arrow highlights a network subset. (G) DAWN analysis: The network illustrates the relationship of clusters, with node indicating the degree of disease association (z-score scale) and node size reflecting cluster size (number of categories).

highlighting efficient memory usage. The scalability of the CWAS-Plus package was tested for run with an increasing number of samples (Fig. 2B, Supplementary Table 2) and datasets (Fig. 2C, Supplementary Table 3). The results revealed a linear increase in execution time with each additional 400 samples, requiring 15 min. Similarly, adding a new functional annotation increased the time by ~6 min. Additionally, we examined the memory usage of CWAS-Plus with an increasing number of samples and found an approximately linear increase (Supplementary Fig. 2). Collectively, these results demonstrated that CWAS-Plus exhibits linear scalability with data size. Notably, CWAS-Plus can handle over 27 000 comparisons with ~4000 samples in 3 h, highlighting its efficiency.

CWAS-Plus also provides an efficient approach to finding the number of effective tests for multiple testing corrections. To accomplish this, CWAS [24] utilized 10 000 sets of random variants. The P-values of the association tests, calculated from each variant set, were then used to measure the correlation between tests (categories). Considering that each variant set requires the same amount of time and memory resources for a single CWAS-Plus execution, this analysis incurs substantial computational costs. Regarding this issue, CWAS-Plus offers a correlation-based method, saving substantial time compared to the former. Both methods cluster categories based on correlation values, yet the correlation-based method calculates the correlation using the number of variants (or samples, in sample-level analysis) shared between two categories. Therefore, the method is fast and effective.

For validation, we compared the outcomes from both methods (Fig. 2D). We observed that the number of clusters in random variant clustering ($n = 2477$) was greater than that in correlation clustering ($n = 1477$). Additionally, we found a higher prevalence of larger clusters (more categories per cluster) in correlation clustering than in random variant clustering (Fig. 2E). These

observations collectively suggest that small clusters in random variant clustering may merge into a single cluster within the correlation clustering approach.

Subsequently, we examined whether multiple clusters from random variant clustering (random variant cluster) converged to a larger cluster in correlation clustering (correlation cluster). Quantifying cluster similarities identified three scenarios: converged, diverged, and concordant. The converged clusters, wherein multiple random variant clusters merged into a single correlation cluster, constituted 67.1% of all random variant clusters (Fig. 2F). Conversely, the diverged clusters, in which a random variant cluster split into multiple correlation clusters, accounted for 18.4%. This observation implies that, in most instances, random variant clusters converged toward a single correlation cluster.

Taken together, these results indicate that the number of correlation clusters is smaller than that of random clusters because random clusters merge into correlation clusters. However, the composition of categories within each cluster remains fairly similar, as correlation clusters absorb small random clusters. Overall, our results demonstrate that the correlation-based method effectively replaces the utilization of random variant sets, considerably reducing computational time and memory usage.

Application of CWAS-Plus to regulatory association in cell-type-specific functional data

Ongoing efforts have been made to generate various annotation datasets for functional regions in the noncoding genome or regulatory enhancers of various cell types and tissues. CWAS-Plus facilitates CWAS analysis by incorporating a new annotation dataset and seeking an appropriate multiple comparison level. Here, we performed the CWAS analyses for *de novo* variants in ASD cases ($n = 4354$) and their unaffected siblings ($n = 2926$) and examined noncoding associations of ASD in cell-type-specific regulatory elements. For this, we obtained various functional datasets,
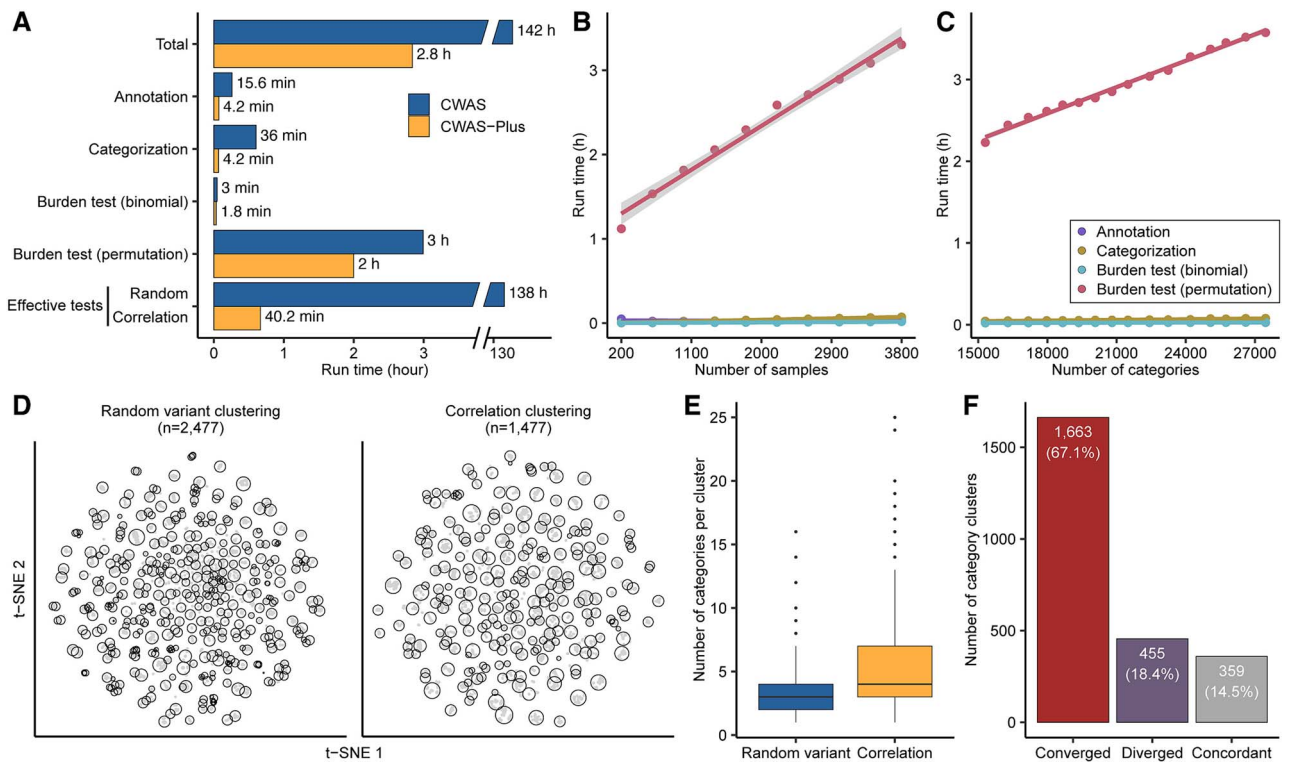
Figure 2. Benchmarking of CWAS-Plus. (A) Comparison of run time between CWAS [24] and CWAS-Plus. Run time was measured using identical annotation datasets and computing resources (3804 samples, 27 462 categories). The y-axis shows each CWAS-Plus step, the x-axis shows run time (h), and numbers next to bars indicate run time per step. (B) Regression line showing execution time with increasing sample size. Dots are observed times, colors represent CWAS-Plus processes, and the gray shade is the confidence interval. (C) Regression line showing execution time with increasing category number. Dots are observed times, colors represent CWAS-Plus processes, and the gray shade is the confidence interval. (D) t-SNE plots displaying the clustered features from random variant clustering and correlation clustering methods. (E) Distribution of the number of categories within each cluster using random variant and correlation clustering methods. The y-axis shows the number of categories per cluster. (F) Comparison of clusters from random variant clustering to correlation clustering. The y-axis shows random variant clusters, the x-axis shows types of differentiation (convergence, divergence, concordant). Convergence/divergence indicates merging/splitting of clusters; concordant indicates alignment of clusters. (A–C) Overall application of CWAS and CWAS-Plus was performed with 36 CPUs and 256 GB RAM.

including single-nucleus ATAC-seq (snATAC-seq) datasets [3, 38–40] from early developmental stages of the human brain (a total of 111 annotation datasets) (Fig. 3A).

Our CWAS analysis generated 142 498 categories for burden testing. As none of the noncoding categories exhibited study-wide significance ($P < 1.4 \times 10^{-5}$), we applied risk score analysis to measure noncoding associations from multiple categories of each genomic region. The results showed that noncoding, including intergenic ($R^2 = 0.20\%$, $P = 1.3 \times 10^{-2}$; Supplementary Tables 4 and 5) and 5' UTR ($R^2 = 0.15\%$, $P = 1.1 \times 10^{-2}$), categories were significantly enriched (Fig. 3B). The performances were prominent after feature selection, indicating its necessity for enhancing model performance. We also performed burden shift analysis and found case-enrichment in intergenic categories ($P = 1.0 \times 10^{-4}$), supporting the association found from risk score analysis (Fig. 3C).

We further explored intergenic variants through DAWN analysis, aiming to identify subnetworks within categories and find risk variants. Leveraging the correlations between categories, a network of intergenic categories was constructed (Fig. 3D). We identified eight clusters associated with ASD (FDR < 5.0×10^{-2}). Clusters of constrained loci, conserved loci, and ASD-associated transcriptional regulator binding sites were densely connected, offering insights into the potential regulatory connections governing these loci.

To examine cluster characteristics, we identified annotation datasets correlated with the clusters. The results revealed cell-type-specificity in clusters 50, 60, and 42, where the former two

clusters were highly correlated with medial ganglionic eminence-derived cells and the latter correlated with astrocytes (Fig. 3E). By contrast, cluster 19 was specific to binding sites targeted by ASD-associated transcriptional regulators [41]. As shown in clusters 19 and 42, ASD associations were also found in evolutionarily conserved elements and regulatory elements specific to fetal brains, consistent with previous findings [42–44]. The results also provided shared features among datasets at the variant level. Specifically, excitatory neuron-CREs (CREs) in early stages were grouped, suggesting more specificity compared to late stages.

We defined variants within significant clusters as RNVs. To validate our results, we utilized a deep-learning prediction tool, Sei [35], to assess the regulatory activities of RNVs. Our observations revealed that variants from most clusters exhibited a higher percentage of variants in higher score bins than non-RNVs (Supplementary Fig. 3), indicating that CWAS-Plus prioritized more pathogenic variants within the broader pool of non-coding variants.

While investigating the role of RNVs in ASD, we hypothesized that RNVs may not only affect the binding sites of transcription factors but also affect transcription factors themselves, thereby disrupting transcriptional regulation. We utilized a list of human transcription factors [34] to conduct enrichment analysis on both RNV-affected and non-RNV-affected genes. The results demonstrated significant enrichment in RNV-affected genes across most clusters compared to that in other noncoding variants (Fig. 3F). Additionally, the transcription
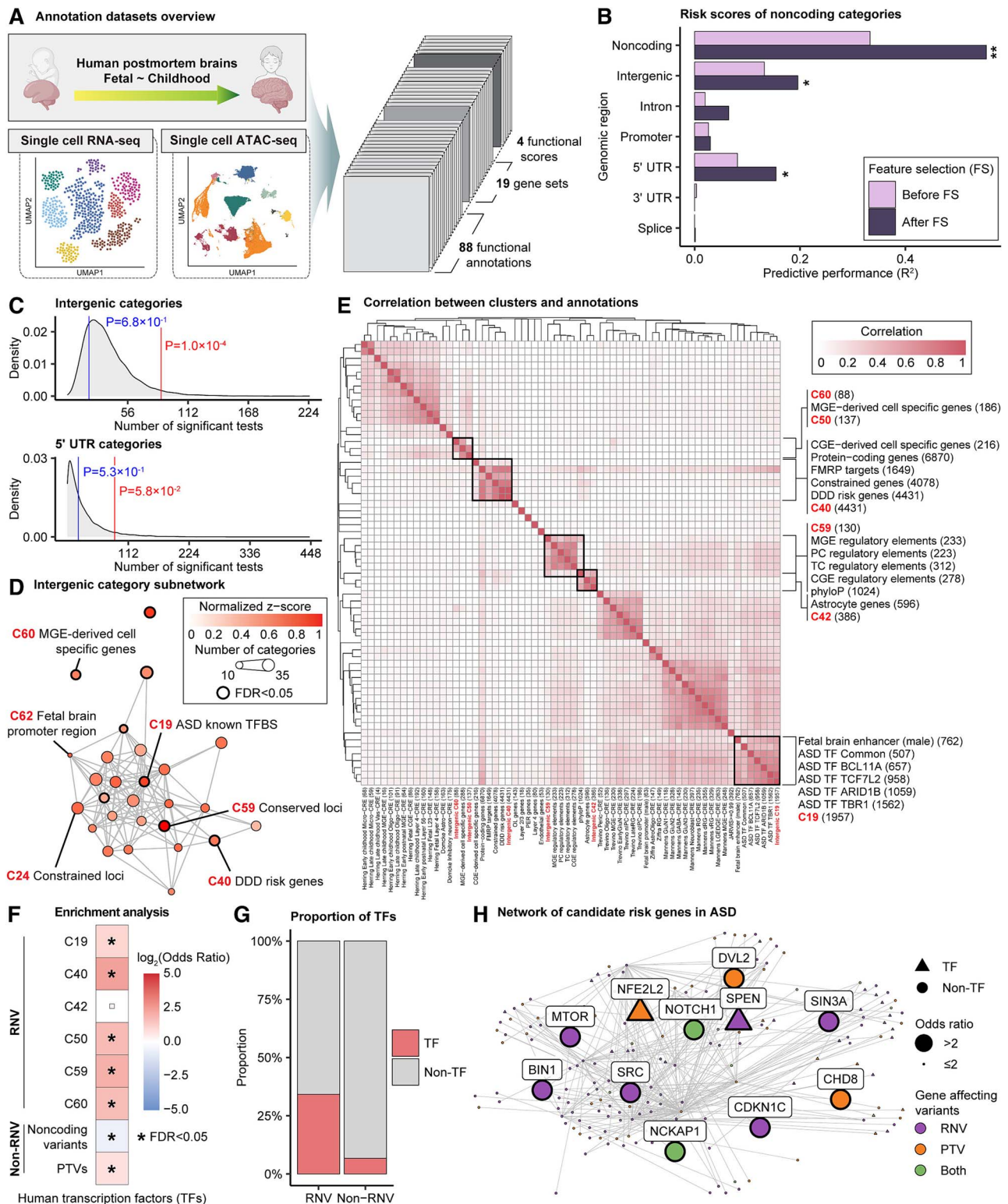
Figure 3. Noncoding association with ASD in cell-type-specific regulatory elements. (A) Summary of annotations for the CWAS analysis for ASD. Created with BioRender.com. (B) Risk score analysis noncoding genomic regions using Lasso regression model. The *x*-axis shows model performance (R^2). Asterisks indicate permuted *P*-values (∗, $P < 5.0 \times 10^{-2}$; ∗∗, $P < 1.0 \times 10^{-2}$). Bars indicate whether feature selection was applied. (C) Burden shift analysis results for intergenic and 5′ UTR categories. Density plots represent the null distribution. Vertical lines show observed significant tests for cases and controls. (D) DAWN analysis results for intergenic categories. Each dot represents a cluster, with disease association shown by normalized *z*-scores. Node size indicates the number of categories in a cluster. Edges represent *P*-value correlation between clusters. Thick borders indicate clusters with FDR $< 5.0 \times 10^{-2}$. (E) Correlations between clusters and single annotations. Degree of correlation between clusters and single annotations is shown. Thick boxes highlight highly correlated annotations. (F) Enrichment analysis results with transcription factors. Significance indicated by asterisks (FDR $< 5.0 \times 10^{-2}$). Boxes show odds ratio. (G) Comparison of the percentage of transcription factors in genes affected by RNVs and non-RNVs. Portions of transcription factors and others are shown. (H) Protein–protein interaction network of genes in transcription regulation pathway and also carry RNV or PTV. Node shapes indicate transcription factors (triangles) or others (circles). Node sizes show odds ratio, and the type of variants carried by the gene are represented.

factors [34] showed five-fold enrichment in RNVs compared to non-RNVs (Fig. 3G), indicating the disruptive influence on gene expression through interference with transcription factor activity.

To understand the regulatory network affected by RNVs, we constructed a protein–protein interaction network involving genes affected by both RNVs and PTVs (Fig. 3H). This network specifically focused on genes involved in transcription regulation. Genes with a high OR for carrying *de novo* variants in ASD cases (OR > 2) showed associations with neurodevelopmental risk. For example, *NCKAP1*, crucial for neuronal differentiation, is implicated in ASD and neurodevelopmental delay [45, 46]. Additionally, *CDKN1C*, exclusively pinpointed by RNVs, was previously reported as a neurodevelopmental risk gene [46]. These findings support the reliability of our analyses, providing insights into potential associations of risk genes regulated by noncoding variants.

Furthermore, we evaluated the advancements of CWAS-Plus in prioritizing disease-specific risk variants by comparing it with other noncoding analysis tools: Sei [35], Enformer [36], and STAARpipeline [22]. Using the same *de novo* variants as in Fig. 3, we compared the OR of variant carriers in case–control samples. CWAS-Plus demonstrated significant case enrichment (OR = 1.3; $P = 5.7 \times 10^{-3}$, 95% CI: 1.1–1.6), while Sei, Enformer, and STAARpipeline showed no significant case enrichment (Supplementary Fig. 4, Supplementary Table 6). These results suggest that CWAS-Plus excels in identifying phenotype-specific variants compared to other tools, highlighting its advantages in analyzing disease associations in noncoding variants.

Application of CWAS-Plus to sample-level analysis of rare variants associated with Alzheimer's disease

While the CWAS framework was mainly developed to test non-coding associations for *de novo* variants, it can be applied to rare variants [23]. For burden tests, the CWAS-Plus package provides a 'sample-level test', estimating case–control association by comparing the number of samples carrying rare variants in each category (Fig. 1C). Unlike *de novo* variants, the number of rare variants is highly variable across individuals due to different genetic backgrounds, potentially leading to spurious genetic associations with the variant-level test. Thus, the CWAS analysis for rare variants should be performed using the sample-level test to yield robust signals.

We evaluated the performance and reproducibility of the sample-level test results against the variant-level test using *de novo* variants. CWAS analyses for *de novo* variants showed highly consistent estimates between the variant-level and sample-level tests (Supplementary Fig. 5, Supplementary Table 7). Given these results, we infer that sample-level tests similarly capture associations as variant-level tests.

With the objective of demonstrating the ability of CWAS-Plus to assess noncoding risk in other genomic disorders, we applied the sample-level test to rare variants in 734 AD cases and 353 controls from ROSMAP WGS data. Annotation datasets included AD-specific CREs [47] and differentially expressed genes from single-cell data [48]. Among 56 728 categories, none reached study-wide significance ($P < 4.9 \times 10^{-5}$). Since no single category fully explained AD risk associated with rare noncoding variants, we conducted a risk score analysis to identify predictors among diverse categories (Fig. 4A, Supplementary Tables 8 and 9). Noncoding categories, including intergenic ($R^2 = 1.26\%$, $P = 4.3 \times 10^{-2}$), intron ($R^2 = 1.67\%$, $P = 3.8 \times 10^{-2}$), and 3′ UTR

($R^2 = 1.51\%$, $P = 7.0 \times 10^{-3}$), were significant, suggesting potential AD risk in these categories.

Focusing on 3′ UTR variants, we applied DAWN analysis and found six significant clusters (FDR < 5.0×10^{-2}), defining variants in the cluster as RNVs for AD (Fig. 4B). To delineate the distinctive features of this cluster, we identified single annotations highly correlated with the clusters (Fig. 4C). The clusters showed enrichment with microglia-specific CREs and constrained loci, indicating the regulatory roles of RNVs in microglia-specific pathways. The microglia signals underscore the robustness of CWAS analysis, given the well-established disruption of neuroinflammatory pathways in AD pathology [49].

We evaluated gene recurrence in 705 cases with RNVs, identifying 82 genes in more than five AD cases (OR > 1) and providing a candidate list for AD risk genes regulated by RNVs (Fig. 4D). Among these, *SMPD3* emerged as a significant recurrent risk gene [OR = Inf; $P = 2.0 \times 10^{-2}$, 95% confidence interval (95% CI): 1.2–Inf]. *SMPD3* encodes the enzyme neutral sphingomyelinase-2, which is significantly reduced in AD cases [50]. Deficiency of *SMPD3* disrupts Golgi lipid remodeling, leading to the accumulation of neurotoxic proteins (APP, Aβ, and pTau), dysproteostasis, and cognitive impairment [51]. Furthermore, *SMPD3* regulates exosome production, which is essential for tau propagation [52]. Inhibiting *SMPD3* reduces tau spread, highlighting its potential as a therapeutic target for AD.

Additionally, we identified *SCD* as a significant recurrent gene in AD (OR = Inf; $P = 2.0 \times 10^{-2}$, 95% CI: 1.2–Inf). *SCD* encodes stearoyl-CoA desaturase, a key enzyme in fatty acid metabolism. *SCD* is pivotal in AD pathogenesis by regulating lipid metabolism, immune responses, and synaptic functions [53]. Inhibition of *SCD* has demonstrated restoration of synaptic density and structure, reduction of microglial activation, and improvement in cognitive outcomes in AD models, positioning it as a promising therapeutic target for AD. These findings validate CWAS-Plus in capturing reliable signals from rare variants and provide insights into potential therapeutic targets.

Utilizing large annotation datasets improves model performance in risk score analysis

One of the key questions in risk score analysis is whether adding more annotation datasets enhances the model's performance. We compared three sets of annotation datasets: set 1, set 2, and set 3 (Fig. 5A). Set 3 corresponds to the initial annotation dataset from Fig. 3A (286 functional annotations and scores; 142 498 categories). Sets 1 and 2 share the same datasets as set 3 but differ in functional annotations. Set 1 includes CREs from Herring *et al.* [3] (20 functional annotations and scores; 48 680 categories), while set 2 expands from set 1 by adding regulatory elements from the Roadmap Epigenomics project [54] and VISTA [55], and binding sites for ASD-associated transcription regulators [41] (274 functional annotations and scores; 69 702 categories).

The introduction of additional regulatory elements improved the model's performance within noncoding categories. Set 3 showed the highest performance, outperforming set 1, followed by set 2 ($R^2 = 0.08\%$, $P = 5.5 \times 10^{-1}$ for set 1; $R^2 = 0.17\%$, $P = 4.3 \times 10^{-1}$ for set 2; $R^2 = 0.33\%$, $P = 3.7 \times 10^{-1}$ for set 3; Fig. 5B, Supplementary Table 10). While certain genomic regions, such as 5′ UTRs, exhibited improved model performance compared to set 1, others, like 3′ UTRs, demonstrated a decrease. These observations emphasize the importance of not only increasing the quantity of annotations but also the composition of the added features to enhance the performance.
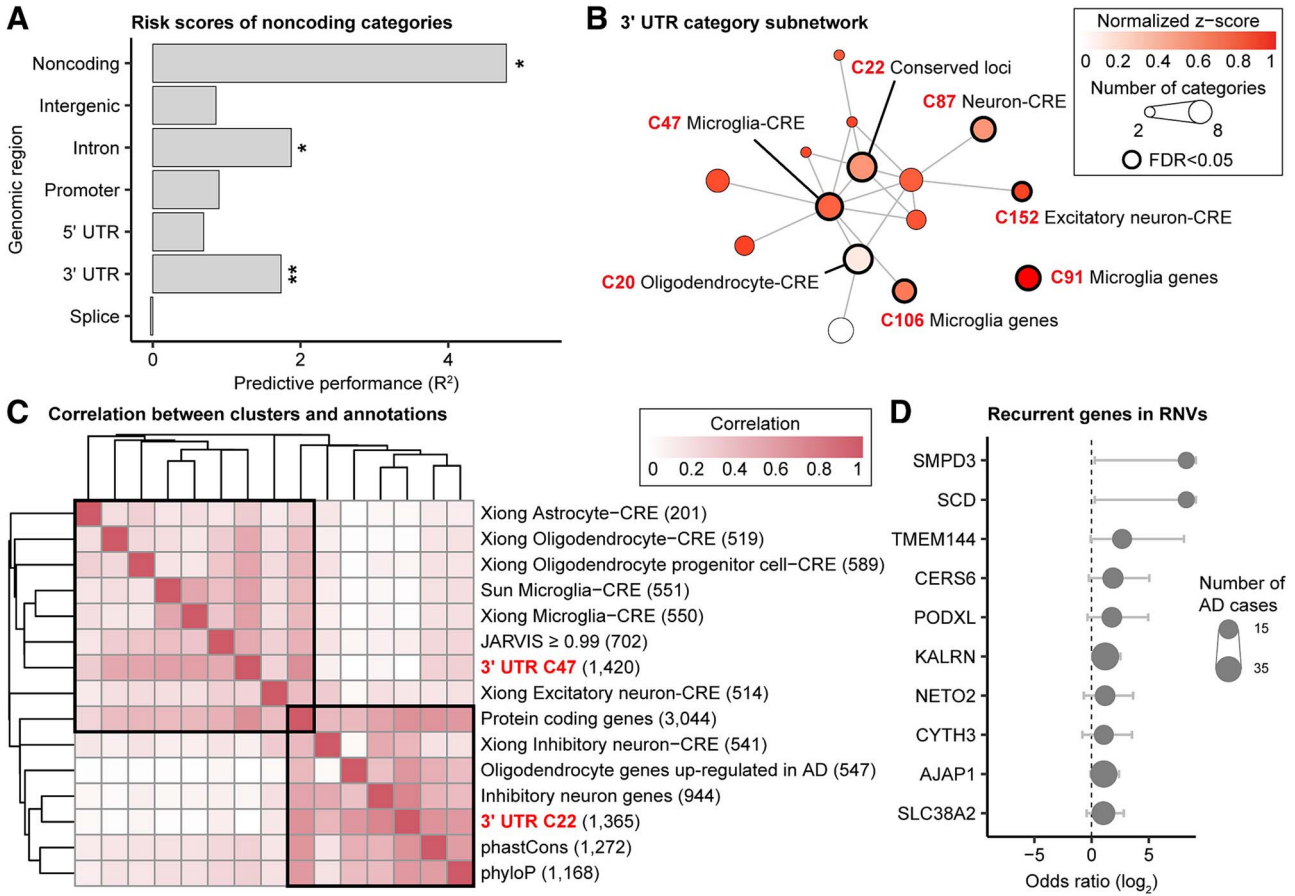
Figure 4. Application of CWAS-Plus to rare variants in Alzheimer's disease. (A) Risk score analysis results of noncoding genomic regions. The x-axis indicates the model performance (R^2) obtained from the lasso regression model. The asterisks indicate permutated p-values ($*$, $P < 5.0 \times 10^{-2}$; $**$, $P < 1.0 \times 10^{-2}$). (B) DAWN analysis results with 3' UTR categories. Each dot represents a single cluster. The degree of disease association is shown by the color of clusters scaled with normalized z-scores. The node size indicates the number of categories within a cluster. The edge refers to the P-value correlation between clusters. The thick borderline indicates clusters with FDR $< 5.0 \times 10^{-2}$. (C) Correlations between clusters and single annotations. The degree of correlation is shown by color. (D) Genes recurrent in RNVs. The x-axis indicates the odds ratio in a $\log_2$ scale. The circle size shows the number of AD cases.
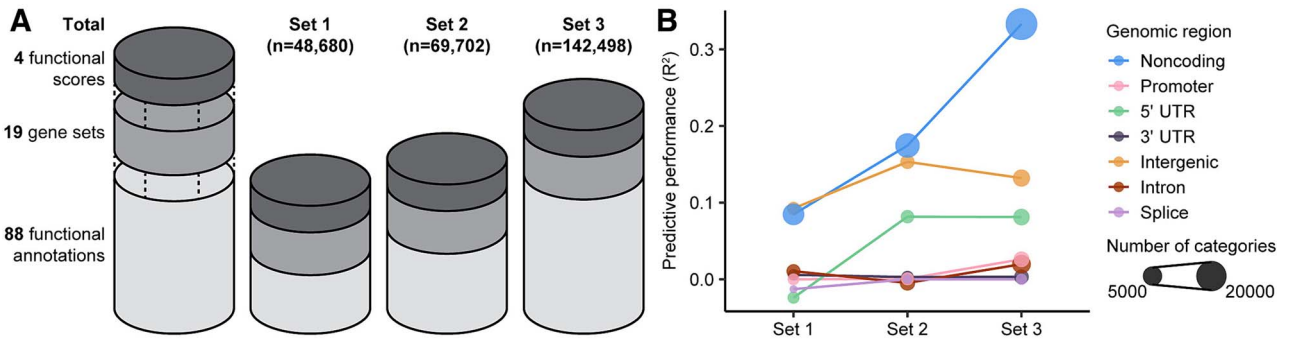
Figure 5. Improved model performance with expanded annotation datasets. (A) A schematic view of three annotation datasets with increasing size. The number of categories is denoted in each set. (B) Model performance of categories from each genomic region in each set from (A). The colors correspond to genomic regions, and the size of data points reflects the number of categories.

Discussion and conclusion

In this study, we introduce CWAS-Plus, a tool for efficient CWAS analysis to identify noncoding associations from WGS data. The package supports user-friendly functions for categorization and burden enrichment tests for various functional datasets. Our tool facilitates the identification of the number of effective tests across multiple tested categories for multiple testing corrections.

Consequently, it is applicable to WGS studies of various human disorders.

Here, we integrated multiple functional datasets, including snATAC-seq datasets from the human cortex, for CWAS analysis of *de novo* variants in ASD families, demonstrating cell-type-specific context for noncoding association. Significant associations were observed in intergenic categories enriched

with regulatory regions of fetal brains and binding sites of ASD-associated transcription regulators. These results suggested that RNVs may contribute to ASD neurobiology by disrupting transcription factors during fetal brain development. Moreover, consistent with our previous finding [24], RNVs were highly correlated with sequence conservation, indicating ASD noncoding association for regulatory elements with evolutionary conservation. Overall, CWAS-Plus enables the integration of accumulated functional datasets with WGS data, thereby facilitating the identification of novel associations between regulatory elements and noncoding variants.

Our extended analysis comparing the ability to identify risk variants revealed that only CWAS-Plus demonstrated significant case enrichment in risk variant carriers, whereas Sei, Enformer, and STAARpipeline did not (Supplementary Fig. 4). This discrepancy may be due to the lack of phenotype consideration, and the limited scope of single-cell and disease-relevant datasets in pretrained models of deep learning tools. While retraining models with custom datasets could enhance accuracy, it is computationally intensive. CWAS-Plus addresses these limitations by integrating multiple functional datasets, including single-cell regulatory datasets, in a time-efficient manner.

STAARpipeline, which also considers phenotype information and utilizes multiple functional datasets, focuses on narrowly defined regions with gene-centric testing and sliding window analysis. The sparse de novo variants and extensive multiple testing burden in the STAARpipeline led to no significant associations, as the tests did not meet genome-wide significance. In contrast, CWAS-Plus's comprehensive approach allows it to identify risk variants with smaller effects by aggregating associations across diverse categories and regulatory elements throughout the genome.

CWAS-Plus provides a novel approach to assessing the genome-wide significance of rare noncoding variants. Unlike GWAS, which estimates effective association tests based on locus correlation, CWAS-Plus addresses the absence of standardized criteria for closely related association tests in rare variants by introducing a method to calculate associations between tests (categories). This unique methodology enables CWAS-Plus to conduct correction for multiple hypothesis testing, providing a tailored significance threshold for rare variants.

CWAS-Plus offers a comprehensive approach to perform analyses at both the variant-level and sample-level. De novo variants occur at a relatively consistent rate across individuals. By contrast, rare variants show higher variability in occurrence rates due to genetic ancestry. CWAS-Plus considers these characteristics and provides both variant- and sample-level tests, allowing its application to de novo and rare variants effectively. Applying CWAS-Plus to rare variants of the AD cohort, despite the limited sample size, revealed potential risks associated with 3′ UTR variants in microglia-specific CREs. These results are consistent with previous findings where microglia-expressed genes were enriched with candidate causal genes found in GWAS [56–58]. Taken together, our findings emphasize the reliability of CWAS-Plus and support the applicability to rare variants and complex genomic disorders, such as AD.

Despite various advantages, our package has a few limitations. CWAS-Plus enables users to customize annotation datasets for their phenotype of interest. However, the degree of freedom may pose challenges for diseases for which there is no access to relevant datasets or clear hypotheses for constructing customized categories. To address this issue, we provide datasets, such as putative promoter and enhancer regions, as a baseline to facilitate a more accessible starting point. Moreover, CWAS-Plus offers feature selection to select phenotype-relevant datasets, refining annotation dataset composition. Furthermore, CWAS-Plus has significantly improved computational speed; however, computation testing at a cohort level with hundreds of thousands of samples has not yet been carried out. Continuous development efforts will be undertaken to overcome these limitations of CWAS-Plus.

In summary, we present CWAS-Plus, a Python package for performing genome-wide assessments of noncoding associations. CWAS-Plus offers an efficient and user-friendly approach for integrating functional datasets with large-scale WGS data and empowers multiple testing comparisons. Our package is applicable to both de novo and rare variants. In future studies, we aim to optimize resource usage for efficient execution, especially in environments with limited memory and computing power. We also plan to utilize additional functional datasets to enhance the identification of regulatory signals, such as topologically associating domains and 3D chromatin interaction datasets. Additionally, we will extend the applicability of CWAS-Plus to various fields, facilitating the exploration of noncoding associations in diverse diseases such as cancers. With CWAS-Plus, we expect to uncover novel noncoding associations and enhance our understanding of genetic contributions to pathologies.

Key Points

- CWAS-Plus efficiently identifies noncoding associations in WGS data, supporting user-friendly categorization and burden enrichment tests.
- CWAS-Plus integrates various functional datasets, emphasizing cell-type-specific noncoding associations.
- CWAS-Plus provides a novel approach for multiple testing correction, enhancing the reliability of the results.
- Autism spectrum disorder risk noncoding variants are identified as enriched with transcription factors, suggesting their role in the pathology.
- Rare variant analysis with Alzheimer's disease samples reveals strong a association with microglia, supporting the reliability of the results produced by CWAS-Plus.

Acknowledgements

Chicago. Data collection was supported through funding by NIA grants P30AG10161 (ROS), R01AG15819 (ROSMAP; genomics and RNAseq), R01AG17917 (MAP), R01AG30146, U01AG32984 (genomic and whole exome sequencing), U01AG46152 (ROSMAP AMP-AD, targeted proteomics), U01AG61356 (whole genome sequencing, targeted proteomics, ROSMAP AMP-AD), the Illinois Department of Public Health (ROSMAP), and the Translational Genomics Research Institute (genomic). Additional phenotypic data can be requested at www.radc.rush.edu.

Supplementary data

Supplementary data are available online at *Briefings in Bioinformatics* online.

Funding

Data availability

The source code of CWAS-Plus is available via a GitHub repository (https://github.com/joonan-lab/cwas/) and Zenodo (https://doi.org/10.5281/zenodo.10795678) [59], with a user manual (https://cwas-plus.readthedocs.io/en/latest/). Both repositories are released under the MIT license. The scripts to produce the annotation dataset, along with the burden test results from the CWAS analyses conducted in this study, are available via Zenodo (https://doi.org/10.5281/zenodo.11240547) [60]. The Zenodo repository is released under the Creative Commons Attribution 4.0 International license. CWAS-Plus is written in Python (version ≥3.9), and is easy to install and use on Linux or Mac OS.

De novo variants were obtained from the pVCF file, accessible with approval from the Simons Foundation Autism Research Initiative (SFARI Base; https://sfari.org/resources/sfari-base). ROSMAP WGS data can be requested at the AD Knowledge Portal under accession code syn10901595 (https://www.synapse.org/#!Synapse:syn10901595; see https://adknowledgeportal.synapse.org/Data%20Access for data access instructions).

Author contributions

Study design: Y.K., M.J., R.Y., D.W., K.R., B.D., S.S., and J.-Y.A. Data processing: Y.K., I.G.K., and H.L. Data analysis: Y.K. Package development: Y.K., M.J., I.G.K., J.H.K., S.S., and J.-Y.A. Manuscript preparation: Y.K., I.G.K., and J.-Y.A. Supervision: S.S., D.W., J.P., I.B.K., and J.-Y.A. All authors have read and approved the final draft of the manuscript for submission.

Ethics approval and consent to participate

References

1. Visel A, Blow MJ, Li Z *et al.* ChIP-seq accurately predicts tissue-specific activity of enhancers. *Nature* 2009;**457**:854–8. https://doi.org/10.1038/nature07730

2. Wu H, Nord AS, Akiyama JA *et al.* Tissue-specific RNA expression marks distant-acting developmental enhancers. *PLoS Genet* 2014;**10**:e1004610. https://doi.org/10.1371/journal.pgen.1004610

3. Herring CA, Simmons RK, Freytag S *et al.* Human prefrontal cortex gene regulatory dynamics from gestation to adulthood at single-cell resolution. *Cell* 2022;**185**:4428–4447.e28. https://doi.org/10.1016/j.cell.2022.09.039

4. Cao J, O'Day DR, Pliner HA *et al.* A human cell atlas of fetal gene expression. *Science* 2020;**370**:eaba7721. https://doi.org/10.1126/science.aba7721

5. Soldner F, Stelzer Y, Shivalila CS *et al.* Parkinson-associated risk variant in distal enhancer of alpha-synuclein modulates target gene expression. *Nature* 2016;**533**:95–9. https://doi.org/10.1038/nature17939

6. Vacic V, McCarthy S, Malhotra D *et al.* Duplications of the neuropeptide receptor gene VIPR2 confer significant risk for schizophrenia. *Nature* 2011;**471**:499–503. https://doi.org/10.1038/nature09884

7. Bae BI, Tietjen I, Atabay KD *et al.* Evolutionarily dynamic alternative splicing of GPR56 regulates regional cerebral cortical patterning. *Science* 2014;**343**:764–8. https://doi.org/10.1126/science.1244392

8. Maurano MT, Humbert R, Rynes E *et al.* Systematic localization of common disease-associated variation in regulatory DNA. *Science* 2012;**337**:1190–5. https://doi.org/10.1126/science.1222794

9. Schaub MA, Boyle AP, Kundaje A *et al.* Linking disease associations with regulatory information in the human genome. *Genome Res* 2012;**22**:1748–59. https://doi.org/10.1101/gr.136127.111

10. Hindorff LA, Sethupathy P, Junkins HA *et al.* Potential etiologic and functional implications of genome-wide association loci for human diseases and traits. *Proc Natl Acad Sci U S A* 2009;**106**:9362–7. https://doi.org/10.1073/pnas.0903103106

11. Watanabe K, Stringer S, Frei O *et al.* A global overview of pleiotropy and genetic architecture in complex traits. *Nat Genet* 2019;**51**:1339–48. https://doi.org/10.1038/s41588-019-0481-0

12. Ritchie GR, Dunham I, Zeggini E *et al.* Functional annotation of noncoding sequence variants. *Nat Methods* 2014;**11**:294–6. https://doi.org/10.1038/nmeth.2832

13. Fu Y, Liu Z, Lou S *et al.* FunSeq2: a framework for prioritizing noncoding regulatory variants in cancer. *Genome Biol* 2014;**15**:480. https://doi.org/10.1186/s13059-014-0480-5

14. Kircher M, Witten DM, Jain P *et al.* A general framework for estimating the relative pathogenicity of human genetic variants. *Nat Genet* 2014;**46**:310–5. https://doi.org/10.1038/ng.2892

15. Huang YF, Gulko B, Siepel A. Fast, scalable prediction of deleterious noncoding variants from functional and population

genomic data. *Nat Genet* 2017;**49**:618–24. https://doi.org/10.1038/ng.3810

16. Zhang S, He Y, Liu H *et al*. regBase: whole genome base-wise aggregation and functional prediction for human non-coding regulatory variants. *Nucleic Acids Res* 2019;**47**:e134. https://doi.org/10.1093/nar/gkz774

17. Ionita-Laza I, McCallum K, Xu B *et al*. A spectral approach integrating functional genomic annotations for coding and noncoding variants. *Nat Genet* 2016;**48**:214–20. https://doi.org/10.1038/ng.3477

18. Quang D, Chen Y, Xie X. DANN: a deep learning approach for annotating the pathogenicity of genetic variants. *Bioinformatics* 2015;**31**:761–3. https://doi.org/10.1093/bioinformatics/btu703

19. Vitsios D, Dhindsa RS, Middleton L *et al*. Prioritizing non-coding regions based on human genomic constraint and sequence context with deep learning. *Nat Commun* 2021;**12**:1504. https://doi.org/10.1038/s41467-021-21790-4

20. Liu Y, Liang Y, Cicek AE *et al*. A statistical framework for mapping risk genes from *de novo* mutations in whole-genome-sequencing studies. *Am J Hum Genet* 2018;**102**:1031–47. https://doi.org/10.1016/j.ajhg.2018.03.023

21. He Z, Xu B, Buxbaum J *et al*. A genome-wide scan statistic framework for whole-genome sequence data analysis. *Nat Commun* 2019;**10**:3018. https://doi.org/10.1038/s41467-019-11023-0

22. Li Z, Li X, Zhou H *et al*. A framework for detecting noncoding rare-variant associations of large-scale whole-genome sequencing studies. *Nat Methods* 2022;**19**:1599–611. https://doi.org/10.1038/s41592-022-01640-x

23. Werling DM, Brand H, An JY *et al*. An analytical framework for whole-genome sequence association studies and its implications for autism spectrum disorder. *Nat Genet* 2018;**50**:727–36. https://doi.org/10.1038/s41588-018-0107-y

24. An JY, Lin K, Zhu L *et al*. Genome-wide de novo risk score implicates promoter variation in autism spectrum disorder. *Science* 2018;**362**:eaat6576. https://doi.org/10.1126/science.aat6576

25. McLaren W, Gil L, Hunt SE *et al*. The Ensembl variant effect predictor. *Genome Biol* 2016;**17**:122. https://doi.org/10.1186/s13059-016-0974-4

26. Kong A, Frigge ML, Masson G *et al*. Rate of de novo mutations and the importance of father's age to disease risk. *Nature* 2012;**488**:471–5. https://doi.org/10.1038/nature11396

27. O'Roak BJ, Vives L, Girirajan S *et al*. Sporadic autism exomes reveal a highly interconnected protein network of de novo mutations. *Nature* 2012;**485**:246–50. https://doi.org/10.1038/nature10989

28. Yurko R, Roeder K, Devlin B *et al*. An approach to gene-based testing accounting for dependence of tests among nearby genes. *Brief Bioinform* 2021;**22**:bbab329. https://doi.org/10.1093/bib/bbab329

29. Liu L, Lei J, Sanders SJ *et al*. DAWN: a framework to identify autism genes and subnetworks using gene expression and genetics. *Mol Autism* 2014;**5**:22. https://doi.org/10.1186/2040-2392-5-22

30. Fischbach GD, Lord C. The Simons simplex collection: a resource for identification of autism genetic risk factors. *Neuron* 2010;**68**:192–5. https://doi.org/10.1016/j.neuron.2010.10.006

31. pfeliciano@simonsfoundation.org SCEa, Consortium S. SPARK: a US cohort of 50,000 families to accelerate autism research. *Neuron* 2018;**97**:488–93. https://doi.org/10.1016/j.neuron.2018.01.015

32. Bennett DA, Buchman AS, Boyle PA *et al*. Religious orders study and rush memory and aging project. *J Alzheimers Dis* 2018;**64**:S161–89. https://doi.org/10.3233/JAD-179939

33. De Jager PL, Ma Y, McCabe C *et al*. A multi-omic atlas of the human frontal cortex for aging and Alzheimer's disease research. *Sci Data* 2018;**5**:180142. https://doi.org/10.1038/sdata.2018.142

34. Lambert SA, Jolma A, Campitelli LF *et al*. The human transcription factors. *Cell* 2018;**172**:650–65. https://doi.org/10.1016/j.cell.2018.01.029

35. Chen KM, Wong AK, Troyanskaya OG *et al*. A sequence-based global map of regulatory activity for deciphering human genetics. *Nat Genet* 2022;**54**:940–9. https://doi.org/10.1038/s41588-022-01102-2

36. Avsec Z, Agarwal V, Visentin D *et al*. Effective gene expression prediction from sequence by integrating long-range interactions. *Nat Methods* 2021;**18**:1196–203. https://doi.org/10.1038/s41592-021-01252-x

37. Li X, Li Z, Zhou H *et al*. Dynamic incorporation of multiple in silico functional annotations empowers rare variant association analysis of large whole-genome sequencing studies at scale. *Nat Genet* 2020;**52**:969–83. https://doi.org/10.1038/s41588-020-0676-4

38. Trevino AE, Muller F, Andersen J *et al*. Chromatin and gene-regulatory dynamics of the developing human cerebral cortex at single-cell resolution. *Cell* 2021;**184**:5053–5069.e23. https://doi.org/10.1016/j.cell.2021.07.039

39. Ziffra RS, Kim CN, Ross JM *et al*. Single-cell epigenomics reveals mechanisms of human cortical development. *Nature* 2021;**598**:205–13. https://doi.org/10.1038/s41586-021-03209-8

40. Mannens CCA, Hu L, Lönnerberg P *et al*. Dynamics of chromatin accessibility during human first-trimester neurodevelopment. *bioRxiv* 2023; 2023.08.18.553878. https://doi.org/10.1101/2023.08.18.553878

41. Darbandi SF, An J-Y, Lim K *et al*. Autism-associated transcriptional regulators target shared loci proximal to brain-expressed genes. *Cell Rep* 2024;**43**:114329. https://doi.org/10.1016/j.celrep.2024.114329

42. Short PJ, McRae JF, Gallone G *et al*. De novo mutations in regulatory elements in neurodevelopmental disorders. *Nature* 2018;**555**:611–6. https://doi.org/10.1038/nature25983

43. Turner TN, Coe BP, Dickel DE *et al*. Genomic patterns of *de novo* mutation in simplex autism. *Cell* 2017;**171**:710–722.e12. https://doi.org/10.1016/j.cell.2017.08.047

44. Turner TN, Hormozdiari F, Duyzend MH *et al*. Genome sequencing of autism-affected families reveals disruption of putative noncoding regulatory DNA. *Am J Hum Genet* 2016;**98**:58–74. https://doi.org/10.1016/j.ajhg.2015.11.023

45. Guo H, Zhang Q, Dai R *et al*. NCKAP1 disruptive variants lead to a neurodevelopmental disorder with core features of autism. *Am J Hum Genet* 2020;**107**:963–76. https://doi.org/10.1016/j.ajhg.2020.10.002

46. Fu JM, Satterstrom FK, Peng M *et al*. Rare coding variation provides insight into the genetic architecture and phenotypic context of autism. *Nat Genet* 2022;**54**:1320–31. https://doi.org/10.1038/s41588-022-01104-0

47. Nativio R, Lan Y, Donahue G *et al*. An integrated multi-omics approach identifies epigenetic alterations associated with Alzheimer's disease. *Nat Genet* 2020;**52**:1024–35. https://doi.org/10.1038/s41588-020-0696-0

48. Mathys H, Peng Z, Boix CA *et al*. Single-cell atlas reveals correlates of high cognitive function, dementia, and resilience to Alzheimer's disease pathology. *Cell* 2023;**186**:4365–4385.e27. https://doi.org/10.1016/j.cell.2023.08.039

49. Kempuraj D, Thangavel R, Natteru PA *et al.* Neuroinflammation induces neurodegeneration. *J Neurol Neurosurg Spine* 2016;**1**:1003.

50. Baloni P, Arnold M, Buitrago L *et al.* Multi-omic analyses characterize the ceramide/sphingomyelin pathway as a therapeutic target in Alzheimer's disease. *Commun Biol* 2022;**5**:1074. https://doi.org/10.1038/s42003-022-04011-6

51. Stoffel W, Jenke B, Schmidt-Soltau I *et al.* SMPD3 deficiency perturbs neuronal proteostasis and causes progressive cognitive impairment. *Cell Death Dis* 2018;**9**:507. https://doi.org/10.1038/s41419-018-0560-7

52. Asai H, Ikezu S, Tsunoda S *et al.* Depletion of microglia and inhibition of exosome synthesis halt tau propagation. *Nat Neurosci* 2015;**18**:1584–93. https://doi.org/10.1038/nn.4132

53. Hamilton LK, Moquin-Beaudry G, Mangahas CL *et al.* Stearoyl-CoA desaturase inhibition reverses immune, synaptic and cognitive impairments in an Alzheimer's disease mouse model. *Nat Commun* 2022;**13**:2061. https://doi.org/10.1038/s41467-022-29506-y

54. Roadmap Epigenomics C, Kundaje A, Meuleman W *et al.* Integrative analysis of 111 reference human epigenomes. *Nature* 2015;**518**:317–30. https://doi.org/10.1038/nature14248

55. Visel A, Minovitsky S, Dubchak I *et al.* VISTA enhancer browser–a database of tissue-specific human enhancers. *Nucleic Acids Res* 2007;**35**:D88–92. https://doi.org/10.1093/nar/gkl822.

56. Bellenguez C, Kucukali F, Jansen IE *et al.* New insights into the genetic etiology of Alzheimer's disease and related dementias. *Nat Genet* 2022;**54**:412–36. https://doi.org/10.1038/s41588-022-01024-z

57. Jansen IE, Savage JE, Watanabe K *et al.* Genome-wide meta-analysis identifies new loci and functional pathways influencing Alzheimer's disease risk. *Nat Genet* 2019;**51**:404–13. https://doi.org/10.1038/s41588-018-0311-9

58. Kunkle BW, Grenier-Boley B, Sims R *et al.* Genetic meta-analysis of diagnosed Alzheimer's disease identifies new risk loci and implicates Abeta, tau, immunity and lipid processing. *Nat Genet* 2019;**51**:414–30. https://doi.org/10.1038/s41588-019-0358-2

59. Kim Y, Jeong M, Koh IG *et al.* Category-wide association study (CWAS) package. *Zenodo* 2024. https://doi.org/10.5281/zenodo.8409105

60. Kim Y, Jeong M, Koh IG *et al.* Generation of annotation dataset and burden test results of category-wide association study (CWAS). *Zenodo* 2024. https://doi.org/10.5281/zenodo.11240547